Prediction of the First Normal Stress Difference in Polymer Solutions

BERNARD J. MEISTER and R. DALE BIGGS

The Dow Chemical Company, Midland, Michigan

Shear stress and first normal stress difference data are presented for several polymer solutions undergoing steady shear rates from 1.0 to 100,000 sec.$^{-1}$. The steady shear response is divided into three regions as a function of increasing shear rate. These are the diffusion controlled linear region, a moderate shear rate region where shear controls the entanglement-disentanglement process, and a high shear rate region where aggregation of polymer molecules occurs. The transitions between the three regions are clearly illustrated by using a group designated as the rotation rate function.

A molecular model is derived for the shear controlled region that allows prediction of the first normal stress difference from the viscosity function and one additional constant that depends only on the molecular species. The White-Metzner equation is found to adequately describe the aggregation region at high shear rates.

The industrial rheologist is faced with three pressing problems in the characterization of viscoelastic liquids. These are the development of equipment to measure the parameters of interest, description of the data in mathematical terms of general utility, and application of these equations to problems of interest. Although most processing equipment does not operate in viscometric flow, the simplicity of the flow field makes viscometric flow a logical starting point for any characterization.

It has been shown (*6, 7*) that the shear stress and two independent normal stress combinations are required to characterize the rheological properties of an elastic material in viscometric flow. The two normal stress functions quite often chosen are the difference between the normal stress prevailing in the direction of flow τ_{11} and that in the direction of the shear gradient τ_{22}, and the difference between the normal stress in the direction of the shear gradient τ_{22} and that in the neutral direction τ_{33}. Experimental measurements of the second normal stress difference $\tau_{22} - \tau_{33}$ are currently in dispute so that the two measurements we must rely on for characterization are the shear stress τ_{12} and the first normal stress difference $\tau_{11} - \tau_{22}$.

Unfortunately, the cone and plate rheogoniometer which is most often employed for measurement of normal stresses is limited to moderate shear rates due to its flow geometry. A capillary instrument, the thrust jet, has been used (*22, 23*) but results have not all been deemed reliable. If reliable thrust jet data can be obtained, the measurements can be combined with those from the rheogoniometer to obtain a complete description of the shear stress-shear rate and first normal stress difference-shear rate curves for polymer solutions. The complete characterization of steady shear behavior presents the opportunity to evaluate some of the more popular constitutive equations and to develop some new ones that are more suited to current needs.

MEASUREMENT OF NORMAL STRESSES

Thrust Jet

The thrust jet apparatus employed in this study is similar to that described by Shertzer (*22*). It should suffice to say here that the thrust jet is a device designed to measure the total axial thrust of a fluid issuing from a capillary tube. If the fluid is elastic, the normal stress in the axial direction can be determined from the difference between the experimentally measured thrust and the thrust which an inelastic fluid would exert.

If it is assumed that fully developed laminar flow exists in the capillary up to the exit and that interfacial forces at the tube exit are negligible, the normal stress can be evaluated from the expression

$$T = \int_0^R [\rho u^2(r) - \tau_{11}(r)]\, dA \qquad (1)$$

where T is the thrust and τ_{11} is the normal stress in the axial direction. The normal stress can be evaluated from this expression by either of two general approaches. The equation can be differentiated with respect to the wall shearing stress to obtain the result (*22, 23*)

$$\tau_{11}(R, L) = \rho V^2 \left[\frac{3n'+1}{n'} - 2\int_0^1 \left(\frac{u}{V}\right)^2 \frac{r}{R}\, d\frac{r}{R} \right] - \frac{T}{\pi R^2}\left[1 + \frac{1}{2n'} \frac{d\ln T}{d\ln 8V/D} \right] \qquad (2)$$

where $n' = d \ln \tau_{12}/d \ln (8V/D)$ and V is the average velocity.

The velocity profile integral can be evaluated either by integration of the experimental data or by use of an appropriate flow equation. For the solutions in this study, the flow behavior obeyed the power law sufficiently well to use this model in the evaluation of the integral. For the power law, it can be shown that

$$2\int_0^1 \left(\frac{u}{V}\right)^2 \frac{r}{R}\, d\frac{r}{R} = \frac{3n+1}{2n+1} \qquad (3)$$

where n is the exponent on the shear rate in the power law equation. If the power law model is valid then $n = n'$ and incorporation of Equation (3) in Equation (2) yields

$$\tau_{11}(R, L) = \rho V^2 \left[\left(\frac{3n'+1}{2n'+1} \right) \left(\frac{n'+1}{n'} \right) \right] - \frac{T}{\pi R^2}\left[1 + \frac{1}{2n'} \frac{d\ln T}{d\ln(8V/D)} \right] \qquad (4)$$

It can be shown from the equations of motion that (*22*)

$$(\tau_{11})_r = (P_{11} - P_{22})_r - p(0, L) - \int_0^r (P_{22} - P_{33})\, d\ln r \qquad (5)$$

If it is assumed that the pressure at the center of the exit of the tube $p(0, L) = 0$ and that the second normal stress difference $\tau_{22} - \tau_{33} = 0$, then

$$(\tau_{11} - \tau_{22})_R = (\tau_{11})_R = \rho V^2 \left[\left(\frac{3n'+1}{2n'+1} \right) \left(\frac{n'+1}{n'} \right) \right] - \frac{T}{\pi R^2}\left[1 + \frac{1}{2n'} \frac{d\ln T}{d\ln(8V/D)} \right] \qquad (6)$$

Therefore, by measurement of the axial thrust, the volumetric throughput and the pressure drop, and differentiation of the thrust and shear stress data, the first normal stress difference can be calculated.

The second method of evaluation of the thrust jet data is by direct integration of Equation (1). Again it must be assumed that the pressure at the center of the exit of the tube is zero, and that the second normal stress difference is zero, so that

$$(\tau_{11})_r = (P_{11} - P_{22})_r = (\tau_{11} - \tau_{22})_r \qquad (7)$$

The main disadvantage is that in addition, a functional form for the dependence of the normal stress on the radial distance must be assumed to integrate Equation (1).

The simplest constitutive equation to apply is the White-Metzner expression (*30, 31*), which for viscometric flows is described by

$$\tau_{11} - \tau_{22} = K_M\ \tau_{12}^2 = K_M\ \tau_w^2 \left(\frac{r}{R}\right)^2 \qquad (8)$$

where K_M is a constant. Substitution of Equation (8) and Equation (3) into Equation (1) yields on integration

$$T = \pi\rho V^2R^2\left(\frac{3n+1}{2n+1}\right) - \frac{\pi K_M}{2}\tau_w^2R^2 \qquad (9)$$

This expression can be simplified by substitution of the Newtonian thrust

$$T_N = \frac{4}{3}\pi\rho V^2R^2 \qquad (10)$$

Then

$$\left(\frac{9n+3}{8n+4}\right)\ T_N - T = \frac{\pi K_M}{2}\tau_w^2R^2 \qquad (11)$$

This expression can be shown equivalent to Equation (6) obtained by the differential method for the special case of a fluid which obeys the White-Metzner relation. The advantage of Equation (11) is that it is much more directly calculable from the experimental numbers than Equation (6). However, it suffers from the restriction that it is meaningless if the fluid does not obey the White-Metzner relation. This is easily checked by the linearity of a plot of $(9n + 3/8n + 4)\ T_N - T$ vs. τ_w^2 and the superposition of tubes of different diameters. Similar relations can be derived for other simple constitutive relations but lacking a satisfactory one for all fluids, the differential method is the best approach.

As with most instruments for the measurement of normal stresses, the thrust jet is limited in its range of operation. Because the analysis requires the existence of fully developed laminar flow, the generalized Reynolds numbers must be below 2,000. Any slight flattening of the velocity profile due to incipient turbulence will greatly increase the normal stress calculated from Equation (6) and render the results useless. There also is a limit at low Reynolds numbers for two reasons. In the derivation it has been assumed that the velocity profile in the exit plane is not affected by the relaxing jet. At low flows below generalized Reynolds numbers of 100, this assumption becomes questionable. However, at these low flows the thrust becomes too small to measure with existing equipment so that the theoretical point is only of academic interest except for extremely viscous solutions.

Rheogoniometer

The Weissenberg cone and plate rheogoniometer is one of the standard instruments for the measurement of normal stresses at low shear rates. The first normal stress difference can be determined directly from the integrated normal force exerted by the fluid during rotation of the cone. If it is assumed that the free liquid boundary at the periphery of the gap takes the form of a sphere with the center at the cone apex, the first normal stress difference is given by the total normal force divided by the plate area (*13*).

$$\tau_{11} - \tau_{22} = \frac{2F}{\pi R^2} \qquad (12)$$

Equation (12) is limited to shear rates such that the fluid in the instrument exhibits small inertial effects. At shear rates above approximately 100 sec.$^{-1}$, inertial forces become significant and decrease the observed normal force. This effect has been studied by Greensmith and Rivlin (*10*), and Williams (*32*) and the most satisfactory correction appears to be an experimental one. Theoretically, the inertial force can be shown to be proportional to the density of the fluid, the square of the plate diameter and the square of the rotational speed. However, the actual force exerted is extremely sensitive to slight asymmetries in the experimental apparatus. As inertial forces also occur in Newtonian fluids, the equipment can be calibrated using a Newtonian fluid and an additive correction factor determined which is a function of shear rate. This correction factor is proportional to the density of the fluid being tested. Application of the correction factor to viscoelastic fluids assumes that the flow patterns of the Newtonian and viscoelastic fluids are the same, which is a first-order approximation that can be justified only by the reasonable results obtained.

Application of the experimental correction factor extends the range of operations of the rheogoniometer to shear rates of 3,000 sec.$^{-1}$ which for the polymer solutions studied here is the lower limit of operation of the thrust jet so that a complete description of the shear stress-shear rate and first normal stress difference-shear rate curves can be obtained from the two instruments.

EXPERIMENTAL PROCEDURE

Thrust Jet

The thrust measurement system was first calibrated by using a system of weights which exerted a known axial force on the capillary tube. The individual capillary tubes were then calibrated using a Newtonian oil of known viscosity and density. The average diameters of the capillary tubes were calculated from the pressure drop using the Newtonian oil. The diameters and lengths of the capillary tubes are listed in Table 1. The accuracy of the thrust measuring system could be determined by comparing the measured thrust to that expected due to the axial momentum of a jet having a parabolic velocity profile. The experimental error was less than 2% for thrusts greater than 2g. which indicated that at least for Newtonian fluids, the velocity profile at the tube exit was fully developed.

Table 1. Thrust Jet Tube Dimensions

Tube no. gauge	Diameter, cm.	Length, cm. (pressure tap to exit)
10	0.2715	28.8
14	0.1602	28.9
16	0.1168	28.6

Measurements were made on a 0.50% hydroxyethyl cellulose (HEC) and 0.10, 0.25, and 0.50% solutions of SEPARAN® AP30® polyacrylamide (PAA). Molecular weights estimated from solution viscosity were 1×10^6 for the hydroxyethyl cellulose and 2×10^6 for the polyacrylamide. Both materials were known to have a broad molecular weight distribution but the degree of dispersity was not known. Twenty liters of each solution were prepared by dissolving the proper amount of polymer in 20 liters of deionized water, which was then agitated slowly for 16 hr. The solutions appeared to be stable as properties did not change from day to day. The solutions were forced through the thrust jet capillary by means of nitrogen pressure and the flow rate, pressure drop from the pressure tap to the tube exit and the thrust recorded for approximately fifteen different flow rates in each capillary tube

and each solution. The shear rate range covered by the three tubes was from 4,000 to 100,000 sec.$^{-1}$.

Rheogoniometer

Measurements were made with the cone and plate rheogoniometer on the 0.50% HEC and 0.25 0.50, and 5.0% PAA solutions. All of the data were obtained using a 7.5 cm. cone with a 1.50 deg. cone angle. The instrument was calibrated with a Newtonian oil of density 0.8803 g./cc. so that data could be taken at high shear rates where inertial effects were significant. A correction factor was determined from the oil data to apply to the normal stress data for polymer solutions. At shear rates above 1,000 sec.$^{-1}$, the correction factor was proportional to the square of the shear rate which agrees with the theoretical analysis of Williams (32). Similar to what Williams observed, some deviation from this proportionality occurs at lower shear rates. These correction factors were then multiplied by 1.135 to account for the higher density of the polymer solutions and added to the normal force measurements. By accounting for the inertial effects, reliable data could be obtained for the shear rate range from 1.0 to 3,000 sec.$^{-1}$.

EXPERIMENTAL RESULTS

The shear stress-shear rate and first normal stress difference-shear rates curves for the 0.50% HEC solution are presented in Figure 1. The normal stresses were calculated from Equation (6) by using the point slopes of the plot of τ_w vs. $8V/D$ to determine the flow behavior index n'. The thrust data were also differentiated to determine the quantity $d\ln T/d\ln(8V/D)$. The shear stresses and normal stresses measured using the three capillary tubes could be fitted by the same curve indicating that entrance effects were eliminated and that the pressure at the tube exit was zero. Some incipient turbulence was noted for the highest flow rates in tubes 10 and 14, but this effect was minor. The rheogoniometer data were not recorded at high enough shear rates to meet the thrust jet data but a smooth curve could be drawn connecting the data from the two instruments.

The shear stress and first normal stress difference are plotted as a function of shear rate for the 0.25 and 0.50% PAA solutions in Figure 2. The PAA data are more accurate than the HEC data due to the higher level of normal stresses present in the solution. For these solutions, the shear stress and first normal stress difference for the two tubes could not be directly superimposed due to some shear degradation occurring in the first tube employed. For the 0.25% solution, the solution used in tube 14 was slightly degraded and for the 0.50% solution, the solution

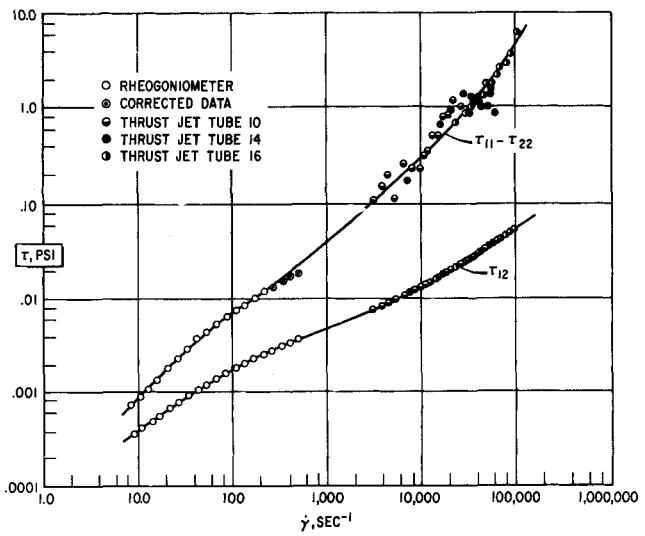

Fig. 1. Shear stress and first normal stress difference data for a 0.50% hydroxyethyl cellulose solution.

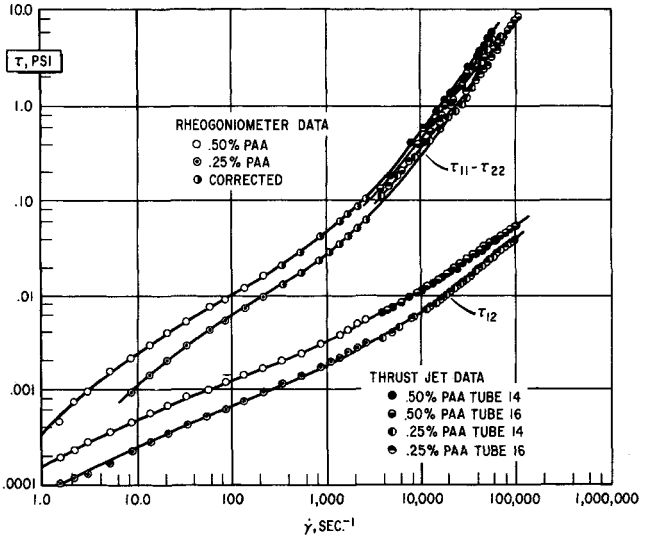

Fig. 2. Shear stress and first normal stress difference data for 0.25 and 0.50% polyacrylamide solutions.

used in tube 16 was slightly degraded. The degradation decreases the elasticity to a greater extent than it does the viscosity. Particularly for the 0.25% PAA, incipient turbulence is observed for the highest shear rates in both tubes. This is indicated by the break in the normal stress curve at a generalized Reynolds number of about 2,000. For the 0.10% PAA solution, turbulence occurred at such low shear rates that no meaningful data could be obtained.

For the 0.25 and 0.50% PAA solutions, the rheogoniometer data were extended to shear rates of 3,000 sec.$^{-1}$ by addition of the inertial correction factor. These points fit excellently with the lower limit of the thrust jet data. The shear stress obtained from the rheogoniometer at high shear rates was slightly in error due to the increased torque caused by the inertial force, but no correction was made for this effect. For both the 0.25 and 0.50% PAA solutions, the rheogoniometer data were obtained on solutions identical in degradation to the tube 14 thrust jet data so it was these curves which were extended to connect the data from the two instruments. The satisfactory meeting of the data from the two instruments lend considerable support to the accuracy of the data obtained from the thrust jet.

CONSTITUTIVE EQUATIONS

Summary of Constitutive Theory and Rheological Models

The focal point of engineering rheology is that of determining a set of simple constitutive equations which will predict the various viscous and elastic phenomena observed experimentally. Such a set of equations could be used directly in process design for simple steady flows and suggest empirical approaches for more complex situations.

The general approaches to the formulation of constitutive equations can be divided into two general formats, the time differential equations and integral equations. The time differential equations are generally presented as either explicit in stress as a function of deformation tensors or explicit in the time derivative of stress. Integral equations are generally explicit in stress as a time integral of the deformation history. Obviously there is a relationship between the forms and many simple models can be formulated either way.

Although most of these theories are formulated in general form, the interest here is in their predictions for viscometric flows, and particularly those equations which apply to polymer solutions. The most important result obtained from theoretical continuum mechanics is that, for a very general class of fluids, only three material functions are required to determine the stresses in a steady visco-

metric flow as shown by Coleman and Noll (*6, 7*). These three functions are generally selected as the viscosity, the primary normal stress difference coefficient, and the secondary normal stress difference coefficient, defined by the following relations:

$$\tau_{12} = \mu\dot{\gamma} \tag{13}$$

$$\tau_{11} - \tau_{22} = \zeta\dot{\gamma}^2 \tag{14}$$

$$\tau_{22} - \tau_{33} = \beta\dot{\gamma}^2 \tag{15}$$

Lacking unambiguous measurements of the second normal stress difference, interest is focused here on predictions of the first two quantities.

The most widely used theory is the linear theory of viscoelasticity, often referred to as a *generalized Maxwell model,* consisting of a series of Maxwell elements connected in parallel. This can be formulated a number of ways but they all lead to the result of a constant viscosity and a constant primary normal stress difference coefficient. This is generally valid for small deformations or low shear rates but most polymer solutions and other highly viscoelastic materials are non-Newtonian at higher shear rates so that the linear theory is extremely limited.

The differential formulation of nonlinear theories was led by Oldroyd (*18*). By formulating the response of the fluid to local shear in a convected coordinate system, the *linear differential* models could be modified by replacing the partial time derivatives by nonlinear convected time derivatives. The results of this analysis were satisfying in that most viscoelastic phenomena could be qualitatively described; however quantitative fitting of the data to the many constants was tedious and not very satisfactory. Bird and coworkers (*11, 24, 25, 33*) have modified the original Oldroyd models to make them simpler to use and more realistic on a molecular basis. Among these models is the three-constant model of Williams and Bird (*33*). The viscosity and primary normal stress coefficient in this model generally decrease too rapidly to satisfy the data. To correct for this, the Spriggs models (*24, 25*) were formulated which employ a distribution of characteristic times to broaden the response curves. The Spriggs four-constant model (*24*) has been one of the most useful of the constitutive equations available. The equations obtained from this model for the steady shear properties are

$$\mu = \frac{\mu_0}{Z(\alpha)} \sum_{n=1}^{\infty} \frac{n^\alpha}{(n^{2\alpha} + c^2\lambda^2\dot{\gamma}^2)} \tag{16a}$$

$$\zeta = \frac{2\lambda\mu_0}{Z(\alpha)} \sum_{n=1}^{\infty} \frac{1}{(n^{2\alpha} + c^2\lambda^2\dot{\gamma}^2)} \tag{16b}$$

$$\beta = \frac{\epsilon\zeta}{2} \tag{16c}$$

Huppler (*11*) employed the form of those models to obtain an empirical model based on the Ellis model viscosity parameters. The predictions of this model fit some steady shear data more satisfactorily than the Williams-Bird and Spriggs models.

White and Metzner (*30, 31*) proposed a generalization of the simple Maxwell model allowing the characteristic relaxation time to be shear dependent. This shear dependence allows the viscosity to vary freely with shear rate, and, in viscometric flows, the normal stress coefficients are given by

$$\zeta = K\mu^2 \tag{17a}$$

$$\beta = 0 \tag{17b}$$

This model requires the viscosity function for the prediction of the normal stresses, but this is not a severe limitation as viscosity data are required in all models to evaluate the constants. For many polymer solutions, the White-Metzner model is a more satisfactory fit to the data than the previous models discussed, particularly at high shear rates. The reasons for this will be discussed later.

The models discussed so far were selected out of a vast number of constitutive equations that have been proposed over the past ten years. All continuum mechanics can do is set restrictions on the allowable forms which these equations can take and the variety of possible forms is infinite as can be seen by recent reviews by Spriggs, Huppler, and Bird (*26*) and Bogue and Doughty (*1*). Ideally one would hope that the form of the equations for a given material could be predicted directly from molecular characteristics. For polymer solutions, these parameters include the molecular weight and molecular weight distribution, the polymer concentration, the flexibility and degree of branching of the polymer molecule, the degree of hydrodynamic interaction between the polymer and solvent, and the solvent viscosity.

The first successful molecular theory was derived by Rouse (*21*) with subsequent modifications by Zimm (*34*), and Bueche (*5*). Three basic assumptions are made in all of these theories. The polymer molecule can be described by a highly flexible segmented chain such that the relative orientations of the segments can be described by a Gaussian distribution. The individual segments, when stressed in a shear field tend to relax to their maximum entropy configuration. The polymer solution is sufficiently dilute so that there are no interactions between the molecules. The molecules are linear and are of uniform molecular weight. The results of Rouse's (*21*) derivation in their simplest form for viscometric flow are:

$$\mu = \mu_s + N_M kT \sum_{s=1}^{N} \lambda_s \tag{18a}$$

$$\zeta = \zeta_s + 2N_M kT \sum_{s=1}^{N} \lambda_s^2 \tag{18b}$$

$$\beta = 0 \tag{18c}$$

where μ_s and ζ_s are the parameters for the pure solvent, N_M is the number of molecules in solution, k is the Boltzmann constant and T is the absolute temperature. Rouse considered the case where there is no hydrodynamic interaction between the polymer and solvent, for which the relaxation time distribution is specified such that

$$\sum_{s=1}^{N} \lambda_s^2 \Big/ \left[\sum_{s=1}^{N} \lambda_s\right]^2 = 0.400 \tag{19}$$

Zimm (*34*) subsequently solved the case where hydrodynamic interaction between the solvent and polymer was great, for which the only change is in the relaxation time distribution and Equation (19) becomes equal to 0.206. These results put the linear theory of viscoelasticity on a firm molecular basis as they predict both a constant viscosity and a constant normal stress coefficient. However application to data can only be made when the rate of deformation is small compared to the longest of the natural relaxation times.

Bueche (*5*) also has undertaken a molecular analysis which again is limited to shear rates where segmental motion is the controlling stress relaxation process. Bueche considers a series of Maxwell elements rotating in a shear gradient and shows that as the shear rate increases the viscous loss per rotation, contributed by the elements, decreases. In this way a non-Newtonian viscosity function is predicted. The viscosity predicted in this way generally decreases much faster with shear rate than the experimen-

tally observed viscosity function. Takemura (27) and Pao (20), using rotating coordinate systems arrive at results similar in form to that of Bueche (5).

There have been several attempts to extend molecular theory to include intermolecular entanglements. Lodge (13, 14) and Mooney (17) both have considered a network of polymer entanglements throughout the solution and have shown that the resulting viscosity and first normal stress coefficient were independent of shear rate. This was a consequence of the assumption that both the number of entanglements and the relaxation time of the entanglements were independent of shear rate. Lodge (13) indicates that the number of entanglements may be a function of shear rate. Gillespie (9) has shown that the Williamson equation for non-Newtonian viscosity can be formulated by assuming the relaxation time to be inversely proportional to shear rate.

The molecular approach appears to be the soundest one for the rheological characterization of materials. The constants obtained in the prediction of the stress functions are more fundamental and can more likely be extended to other materials. Even more significantly, characterization in this way should lead to the ability to tailor-make molecules to achieve desired rheological properties. This is not to belittle the importance of continuum mechanics. It is only that molecular considerations must be incorporated into the formats predicted by continuum mechanics. As both the mathematically general stress formulations and the molecular considerations can become exceedingly complex some approximations must be made in both areas to obtain a workable model.

A Molecular Entanglement Theory for Prediction of Normal Stresses

By using the tensor notation of Lodge (13), the stress tensor for steady shear flows is given by

$$\tau^{ij} = -p_0\,\delta^{ij} + \int_0^\infty \psi(\bar{t}, L_2) \begin{bmatrix} \dot{\gamma}^2\bar{t}^2 & \dot{\gamma}\bar{t} & 0 \\ \dot{\gamma}\bar{t} & 0 & 0 \\ 0 & 0 & 0 \end{bmatrix} d\bar{t} \tag{20}$$

where $\psi(\bar{t}, L_2)$ is the relaxation function and L_2 is the second invariant which for steady shear is the square of the shear rate.

If the polymer solution is considered to be an entangled mass of polymer molecules within a matrix of low viscosity material, each molecular entanglement can be treated as a Maxwell element and the memory function of the gross solution can be treated as a summation of such elements. The word *entanglement* is used rather loosely here and only indicates a contact between two molecules which results in a stress and subsequent relaxation. The spectrum of such possible contacts is broad and the resulting relaxation time distribution is broad. The relaxation function is represented by

$$\psi(\bar{t}, \dot{\gamma}^2) = \sum_{s=1}^{m} \frac{K'_s}{\lambda'_s} e^{-\bar{t}/\lambda'_s} \tag{21}$$

where λ'_s is the relaxation time of a particular entanglement and K'_s is the product of the number of entanglements of relaxation time λ'_s and the spring constant of these entanglements. Relying on the kinetic theory of elasticity, an arbitrary separation is made of the two components into an effective number of entanglements N'_s each having a spring constant kT.

$$K'_s = kTN'_s \tag{22}$$

where k is the Boltzmann constant and T is the absolute temperature. Equivalently

$$\sum_{s=1}^{m} K'_s = kTN'_0 \tag{23}$$

where N'_0 is the total number of effective entanglements/cubic centimeters of solution.

To generalize the memory function completely, the individual relaxation time λ'_s is assumed to be a function of the shear rate

$$\lambda'_s = \lambda_s f_s(\dot{\gamma}^2) \tag{24}$$

and the number of entanglements of relaxation time λ'_s is also assumed to be a function of the shear rate

$$K'_s = K_s g_s(\dot{\gamma}^2) \tag{25}$$

The function $f_s(\dot{\gamma}^2)$ represents the decrease in the relaxation time λ_s of an entanglement due to the forces applied by the shear gradient. The function $g_s(\dot{\gamma}^2)$ represents the change in the number of effective entanglements of relaxation time λ_s at steady state resulting from the shear gradient. Both of these conditions satisfy the requirements of general tensor formulations, that is invariance with regard to the chosen coordinate system, as $\dot{\gamma}^2$ is the second invariant, L_2, for steady shear and may be some other quantity in other situations. The generalized memory function is then

$$\psi(\bar{t}, \dot{\gamma}^2) = \sum_{s=1}^{m} \frac{K_s g_s(\dot{\gamma}^2)}{\lambda_s f_s(\dot{\gamma}^2)} e^{-\bar{t}/\lambda_s f_s(\dot{\gamma}^2)} \tag{26}$$

Substitution of the relaxation function into the stress tensor (20) allows one to integrate directly for the shear stress and normal stresses. The shear stress is given by

$$\tau_{12} = \int_0^\infty \sum_{s=1}^{m} \frac{K_s g_s(\dot{\gamma}^2)}{\lambda_s f_s(\dot{\gamma}^2)} e^{-\bar{t}/\lambda_s f_s(\dot{\gamma}^2)}\, \dot{\gamma}\bar{t}\, d\bar{t} = \dot{\gamma} \sum_{s=1}^{m} K_s g_s(\dot{\gamma}^2)\lambda_s f_s(\dot{\gamma}^2) \tag{27}$$

From Equation (13), the viscosity function is then given by

$$\mu(\gamma^2) = \sum_{s=1}^{m} K_s g_s(\dot{\gamma}^2)\lambda_s f_s(\dot{\gamma}^2) \tag{28}$$

Similarly, the first normal stress difference is given by

$$\tau_{11} - \tau_{22} = \int_0^\infty \sum_{s=1}^{m} \frac{K_s g_s(\dot{\gamma}^2)}{\lambda_s f_s(\dot{\gamma}^2)} e^{-\bar{t}/\lambda_s f_s(\dot{\gamma}^2)}\, \dot{\gamma}^2\bar{t}^2\, d\bar{t} = 2\dot{\gamma}^2 \sum_{s=1}^{m} K_s g_s(\dot{\gamma}^2)\lambda_s^2 [f_s(\dot{\gamma}^2)]^2 \tag{29}$$

and substitution of Equation (28) into Equation (29) yields

$$\tau_{11} - \tau_{22} = \frac{2[\mu(\dot{\gamma}^2)]^2 \dot{\gamma}^2 \sum_{s=1}^{m} K_s g_s(\dot{\gamma}^2)\, \lambda_s^2\, [f_s(\dot{\gamma}^2)]^2}{\left[\sum_{s=1}^{m} K_s g_s(\dot{\gamma}^2)\lambda_s f_s(\dot{\gamma}^2)\right]^2} \tag{30}$$

The second normal stress difference is zero.

If it is assumed that each relaxation time is affected by shear in the same way

$$f_1(\dot{\gamma}^2) = f_2(\dot{\gamma}^2) = f_s(\dot{\gamma}^2) \tag{31}$$

and also that the character of the relaxation time distribution does not change; that is the change in number of en-

tanglements on increasing shear rate will be proportional to the number of entanglements of a given relaxation time already present, then

$$g_1(\dot{\gamma}^2) = g_2(\dot{\gamma}^2) = g_s(\dot{\gamma}^2) \tag{32}$$

Employment of Equations (31) and (32) in Equation (28) yields

$$\mu(\dot{\gamma}^2) = f(\dot{\gamma}^2)\, g(\dot{\gamma}^2) \sum_{s=1}^{m} K_s\lambda_s \tag{33}$$

Substitution of Equations (31) and (32) in Equation (30) yields

$$\tau_{11} - \tau_{22} = \frac{2[\mu(\dot{\gamma}^2)]^2\, \gamma^2 \sum_{s=1}^{m} K_s\lambda_s^2}{g(\dot{\gamma}^2)\left[\sum_{s=1}^{m} K_s\lambda_s\right]^2} \tag{34}$$

As K_s and λ_s are constants, Equation (34) can be expressed as

$$\tau_{11} - \tau_{22} = \frac{K\tau_{12}^2}{g(\dot{\gamma}^2)} \tag{35}$$

Equation (35) is identical to the White-Metzner Equation (8) corrected for the effect of shear on the number of entanglements in the solution. If the effective entanglement density in the solution is constant, Equation (35) is identical to the White-Metzner equation.

Equation (34) can be rearranged to be solved for the shear modulus G:

$$G = \frac{\tau_{12}^2}{\tau_{11} - \tau_{22}} = \frac{g(\dot{\gamma}^2)\left[\sum_{s=1}^{m} K_s\lambda_s\right]^2}{2\sum_{s=1}^{m} K_s\lambda_s^2} \tag{36}$$

Using the symbol E to denote expected value

$$\frac{\left[\sum_{s=1}^{m} K_s\lambda_s\right]^2}{\sum_{s=1}^{m} K_s\lambda_s^2} = kTN_0\,\frac{[E(\lambda_s)]^2}{E(\lambda_s^2)} = kTN_0\Phi \tag{37}$$

The statistical parameter Φ can vary from 1.0 for a monodisperse spectrum down to very small numbers for an extremely broad spectrum. However, for many common distributions, Φ is centered around the value ½. For both an exponential distribution and the standard log normal distribution $\Phi = ½$. For many polymeric materials (29), the intermolecular entanglement portion of the relaxation spectrum is reasonably well represented by the standard log normal distribution.

Assuming a standard log normal distribution in Equation (36) yields the result

$$G(\gamma^2) = \frac{kTN_0\, g(\dot{\gamma}^2)}{4} \tag{38}$$

Equation (38) predicts that the only variable on which the shear modulus depends is the effective number of entanglements per volume of solution. To evaluate this, recourse must be made to molecular considerations. The four physical variables which may affect the number of entanglements are the polymer concentration, the molecular weight of the polymer, the chain stiffness of the molecule, and the rate of shear. The shear dependence has been expressed as $g(\gamma^2)$ in Equation (38) and is a result of two competing factors.

1. As the rate of shear is increased, the individual molecules rotate faster in the shear gradient so that more entanglements are formed per unit time.
2. As the shear rate is increased, the molecules are pulled apart quicker so that more entanglements are broken per unit time. A detailed analysis requires formulation of expressions for the rate of formation and rate of breakage of entanglements.

The mechanism proposed here is that of a freely orienting chain rotating in the shear gradient in an essentially spherical shape and forming entanglements with other molecules on its outer surface due to the rotation of the molecule. If this model is correct, then the rate of formation of entanglements for a given molecule will be proportional to its surface area, its velocity of rotation, and the polymer concentration or the amount of material with which it can entangle.

$$\frac{dN_F}{dt} = k_F N_M R^2 V(\dot{\gamma}^2) C \tag{39}$$

where

N_M is the number of molecules/cc.
R^2 is the square of the effective radius of the polymer molecule, sq.cm.
$V(\gamma^2)$ is the velocity of the surface of the molecule, cm./sec.
C is the polymer concentration, g./cc.

The number of molecules/cc. is given by

$$N_M = \frac{CN_{Av}}{M} = \frac{6 \times 10^{23}\, C}{M} \tag{40}$$

and the velocity of rotation is equal to the rotation rate times the radius

$$V(\gamma^2) = R\ \omega(\dot{\gamma}^2) \tag{41}$$

If the molecule can be assumed to have the dimensions of a freely orienting chain (4), then

$$R^2 \approx 10^{-16}\ M \text{ sq.cm.} \tag{42}$$

For oriented molecules, the dependence of radius on molecular weight may be somewhat greater. Substituting Equations (40), (41), and (42) into Equation (39) yields the following expression for the rate of formation of entanglements

$$\frac{dN_F}{dt} = 0.60\ k_F C^2 M^{0.5}\, \omega(\dot{\gamma}^2) \tag{43}$$

The rate of breakage of entanglements is given simply by the number of entanglements divided by the mean relaxation time. Therefore

$$\frac{dN_B}{dt} = \frac{N_0\, g(\dot{\gamma}^2)}{E[\lambda_s f(\dot{\gamma}^2)]} \tag{44}$$

But from Equation (33), it is seen that

$$E[\lambda_s f(\gamma^2)] = \frac{\mu(\dot{\gamma}^2)}{kTN_0\, g(\dot{\gamma}^2)} \tag{45}$$

Then

$$\frac{dN_B}{dt} = \frac{kT[N_0\, g(\dot{\gamma}^2)]^2}{\mu(\dot{\gamma}^2)} \tag{46}$$

For steady shear, the rate of formation and rate of breakage have attained their equilibrium values, so that

$$\frac{dN_F}{dt} = \frac{dN_B}{dt} \tag{47}$$

Substituting Equations (43) and (46) into Equation (47)

and solving for the number of entanglements yields the final expression

$$N_0\, g(\gamma^2) = \sqrt{\frac{0.60 k_F C^2 M^{0.5}\, \omega(\dot\gamma^2)\mu(\dot\gamma^2)}{kT}} \qquad (48)$$

Equation (48) relates the number of entanglements to the known quantities of concentration, molecular weight, temperature and viscosity. The two unknowns are the constant k_F and the rotation rate.

For a given polymer, k_F should be a constant independent of concentration and molecular weight. It relates the number of entanglements formed to the surface area of the molecule, distance rotated and concentration of polymer in the solution. The constant should mainly depend on the chain stiffness and linearity of the polymer molecule.

The rate of rotation of the polymer molecule is $\omega(\gamma^2)$. At low concentrations and shear rates, when the molecules can rotate freely, the rate of rotation is equal to the shear rate divided by 2 as shown by Bueche (*4*). However, when the effective entanglement density exceeds 1.0, a semipermanent network is formed and the rate of rotation is restricted. Forces will build up in this network and result in either the breaking of the individual molecules (permanent degradation) or aggregation of the molecules into rotating clumps. The latter appears to be more likely and is analogous to the supermolecular rotating rheological units described by Mooney (*17*). If the molecules aggregate into clumps and the entanglements external to the clumps still control the relaxation process, the smaller number of units in the network will cause the calculated number of entanglements per molecule to decrease. However, the increased importance of the relaxation times within the clump relative to the external entanglements will make the theoretical basis of the calculation less meaningful. In fact, if the entanglements absorbed into the rotating unit maintain their energy storage ability, the calculated effective entanglement density will remain constant with increase in shear rate. Lacking a more sophisticated theory, this is probably a reasonable assumption. The result can be expressed as an apparent change in the rotation rate function $\omega(\dot\gamma^2)$ by solving Equation (48) for the case of constant entanglement density. The rotation rate function is then given by

$$\dot\gamma < \dot\gamma_B \quad \nu < 1 \quad \omega(\gamma^2) = \dot\gamma/2 \qquad (49)$$

$$\dot\gamma > \dot\gamma_B \quad \nu = 1 \quad \omega(\gamma^2) = \frac{\dot\gamma_B}{2}\,\frac{\mu(\dot\gamma_B{}^2)}{\mu(\dot\gamma^2)} \qquad (50)$$

where γ_B is the critical shear rate at which a semipermanent network is formed and ν is the effective entanglement density defined by the equation

$$\nu = \frac{N_0\, g(\dot\gamma^2)}{N_M} \qquad (51)$$

In physical terms, the effective entanglement density is the number of entanglements per molecule that act like permanent crosslinks at the shear rate in question. The value of ν increases from zero at zero shear rate to 1.0 at the critical shear rate. The value of ν at which a network is formed will probably be somewhat greater than one as shown by Flory (*8*) because of the distribution of molecular weights and statistical distribution of entanglements in any polymer sample.

Comparison of the predictions of the proposed molecular model with experimental data is best performed by plotting the apparent rotation rate vs. the shear rate. Solving Equation (48) for the rotation rate and substitution of Equation (38) yields for a given polymer species

$$\omega(\dot\gamma^2) = \frac{K[G(\dot\gamma^2)]^2}{C^2 M^{0.5}\,\mu(\dot\gamma^2)\,T} \qquad (52)$$

For shear rates below the critical shear rate γ_B, substitution of Equation (49) yields

$$\frac{[G(\dot\gamma^2)]^2}{\mu(\dot\gamma^2)C^2M^{0.5}\,T} = K_R\,\gamma \qquad (53)$$

and for shear rates above γ_B, substitution of Equation (50) yields

$$\frac{[G(\dot\gamma^2)]^2}{\mu(\dot\gamma^2)C^2M^{0.5}\,T} = K_R\,\gamma_B\,\frac{\mu(\dot\gamma_B{}^2)}{\mu(\dot\gamma^2)} \qquad (54)$$

The characteristic group on the left-hand side of Equations (53) and (54) is designated as the rotation rate function. K_R is a constant that depends on the flexibility of the polymer chain in solution for the particular polymer species-solvent combination. The first normal stress difference can be predicted from knowledge of the constant K_R and the viscosity function. The shear rate at which the transition between Equations (53) and (54) occurs can be calculated from Equations (38), (51), and (53).

$$\dot\gamma_B = \frac{k^2 N_{Av}{}^2\, T}{16 K_R \mu(\dot\gamma_B) M^{2.5}} \qquad (55)$$

Equation (55) predicts that the shear rate at which aggregation occurs decreases sharply with increasing molecular weight and concentration. As an example of the strong dependence predicted, consider a material with a viscosity curve that fits the following equation in the power law region

$$\mu(\dot\gamma^2) = \frac{K\,C\,M^{1.5}}{\dot\gamma^{0.5}} \qquad (56)$$

Substitution of Equation (56) in Equation (55) yields the result

$$\gamma_B = \frac{K\,T^2}{C^2\,M^{16}} \qquad (57)$$

Equation (57) predicts an extremely high dependence of the critical shear rate on molecular weight.

Comparison of Theory with Experimental Data

The data obtained from the 0.50% HEC solution are plotted in the form suggested by Equation (53) in Figure 3. The thrust jet data points are taken from the smoothed curve through the normal stress data of Figure 1. At shear rates below 300 sec.$^{-1}$, the rotation rate increases directly proportional to the shear rate as predicted by the model. At a shear rate of 300 sec.$^{-1}$, an abrupt break occurs in the plot and at higher shear rates Equation (54) represents the data quite adequately. The effective entanglement density at any point on the curve can be calculated from Equations (38) and (51). At $\dot\gamma$ = 10 sec.$^{-1}$, ν = 0.40 entanglements per molecule. At the break point in

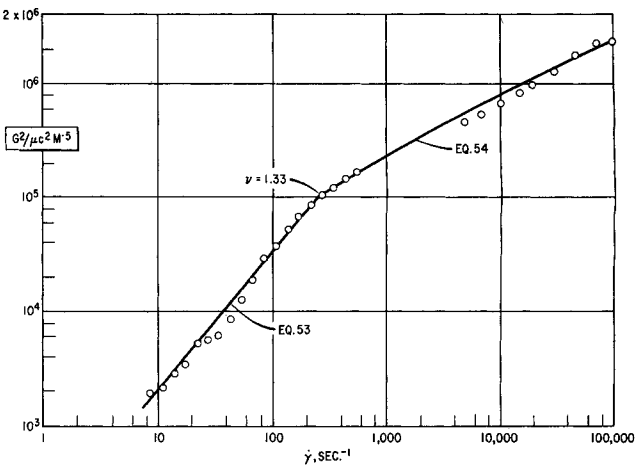

Fig. 3. Rotation rate function calculated from 0.50% hydroxyethyl cellulose solution data.

the curve, the calculated entanglement density is 1.33 entanglements per molecule. This agrees extremely well with the model considering that a value somewhat greater than one was expected due to molecular weight distribution. The calculated entanglement density depends on the *assumption of* a standard log normal distribution of relaxation times and the estimated molecular weight of one million. However, these assumptions do not affect the shape of the plot or the predicted shear dependence.

The data obtained from the 0.25, 0.50 and 5.0% polyacrylamide solutions are plotted in Figure 4. The solid curves are the predictions of the model using the experimental values of K_R and the experimental break point as the transition between two regions. The rotation rate functions for all three solutions are linear with shear rate up to a critical shear rate. The critical shear rates are 1,700, 900, and 35 sec.$^{-1}$ for the 0.25, 0.50 and 5% solutions, decreasing with increasing concentration. The calculated entanglement densities at the break point using the average molecular weight estimate of two million were 1.46, 1.30, and 1.95 respectively. The rotation rate function above the critical shear rate for the two dilute solutions can be adequately described by using Equation (54) for a constant entanglement density. The 5.0% solution cannot be as satisfactorily described, as the calculated entanglement density decreases considerably at shear rates above 35 sec.$^{-1}$. This is possibly an effect of narrowing the relaxation spectrum on increasing shear rate as the natural relaxation spectrum is particularly broad for this concentrated solution. The broad relaxation spectrum may also be the cause of the unusually high calculated entanglement density at the break point. The constant K_R in Equation (53) varied by a factor of four over the twentyfold concentration range. This could either be an effect of degradation or an unaccounted for concentration effect.

Figure 5 shows some of the literature data of Williams (*32*) for a 1.54% HEC solution and an 8.0% polyvinyl alcohol (PVA) solution. Both of these solutions have calculated entanglement densities less than one over the shear rate range studied so that it is expected that the rotation rate function will increase linearly with shear rate. This expectation is confirmed in Figure 5.

No assumptions have been made in the analysis regarding the mean of the relaxation time distribution. From Equations (38) and (45) it is seen that

$$E[\lambda_s f(\dot{\gamma}^2)] = \frac{\mu(\dot{\gamma}^2)}{4G(\dot{\gamma}^2)} \qquad (58)$$

By using Equation (58), the mean relaxation time can be calculated directly from the data. Figure 6 shows the mean relaxation time as a function of shear rate for the 0.50%

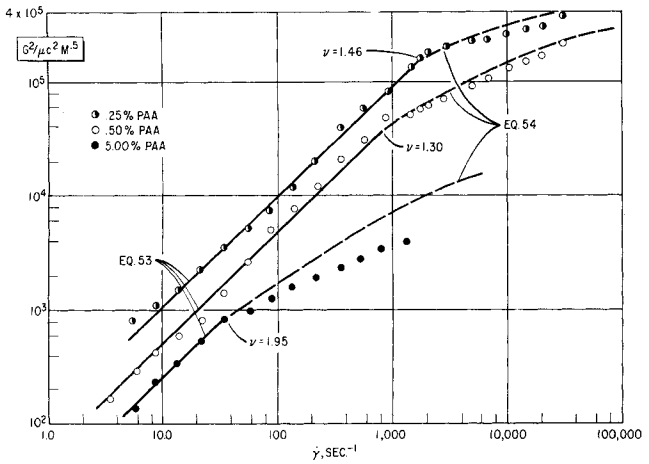

Fig. 4. Rotation rate function calculated from polyacrylamide solution data.

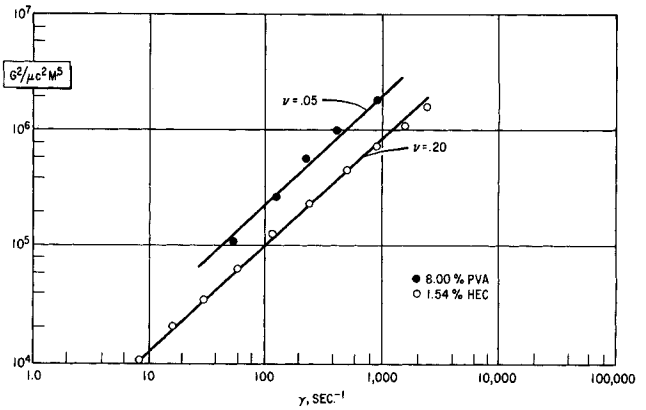

Fig. 5. Rotation rate function calculated from Williams (*32*) data for a 1.54% hydroxyethyl cellulose solution and an 8% polyvinyl alcohol solution.

HEC solution and the three polyacrylamide solutions. The mean relaxation time decreases markedly with increase in shear rate, due to the forces imposed on the entanglement junctions by the shear gradient. These data and some calculations on other data in the literature indicate that the mean relaxation time calculated from the model is independent of concentration and molecular weight in the shear controlled region. This is a significant result as it indicates that when an expression can be formulated for the effect of shear on the mean relaxation time, a complete steady shear characterization can be made in the shear controlled region with constants that are independent of concentration and molecular weight.

Several approaches to describing the effect of shear on the relaxation time have appeared. Gillespie (*9*) and Bogue (*2*) both use the concept of an effective relaxation time

$$\lambda_E = \frac{\lambda}{1 + k\dot{\gamma}\lambda} \qquad (59)$$

thereby modifying the kernel in Equation (20). Tanner (*28*) has accomplished a similar objective by modifying the limits of integration so that after a strain of a certain magnitude the juncture is broken. Both of these approaches can yield plots of the mean relaxation time similar to Figure 6 if the initial relaxation spectrum is broad.

Transition from Diffusion Controlled Relaxation to Shear Controlled Relaxation

All of the data illustrated in the last section were taken in the shear rate range where the effect of shear on the intermolecular entanglements controlled the stress relaxation process. At very low shears, it has been fairly well substantiated that the segmental motion of the individual molecules as described by Rouse (*21*) controls the relaxation process. As long as the shear rate is low compared to the longest relaxation time of the diffusion process, the observed viscosity and first normal stress coefficient are constant.

As the shear rate is increased, a point is reached where the slow segmental diffusion process can no longer relax the stresses imposed by the shear gradient on the intermolecular junctures. Stresses then build up at the juncture and cause more rapid relaxation or disentanglement than would occur by Brownian motion. A decrease of the mean relaxation time as evidenced in Figure 6 was a consequence of this occurrence. It would be desirable to predict the entire stress shear rate curve by one relaxation function involving terms for the natural diffusion process and the modification of this natural process by the imposed shear. This has been done, at least mathematically, in many of the constitutive equations (*2, 24, 32*) by using the Newtonian limit as a reference value. However, in the present

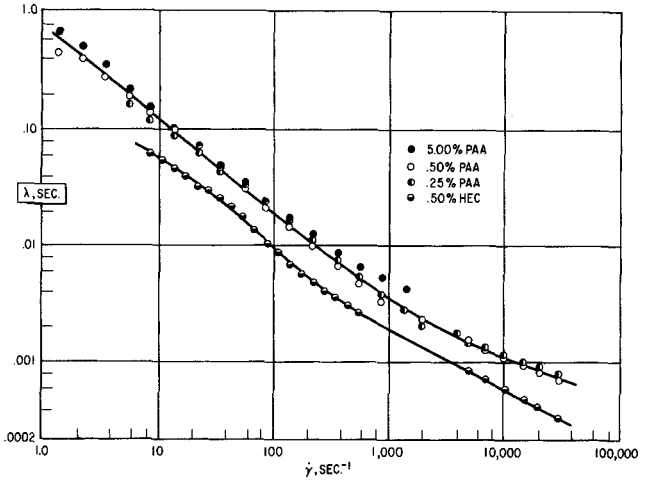

Fig. 6. Mean relaxation times for three polyacrylamide solutions and a hydroxyethyl cellulose solution.

case, the combining of terms can best be done empirically using the characteristic group denoted as the rotation rate function in the shear controlled region. At low shears, where segmental motion controls, the Rouse (*21*) equations can be rearranged to yield

$$\frac{G^2}{\mu C^2 M^{0.5} T} = \frac{K_1}{CM^{1.5}} \qquad (60)$$

At high shears where the shearing motion controls the relaxation spectrum Equation (53) applies, so that at any shear rate

$$\frac{[G(\dot\gamma^2)]^2}{\mu(\dot\gamma^2) C^2 M^{0.5} T} = \frac{K_1}{CM^{1.5}} + K_R \dot\gamma \qquad (61)$$

A plot of the characteristic group vs. shear rate for a particular polymer in the transition range should involve a transition from constants, which depend on the concentration and molecular weight, to a linear relationship which is independent of concentration and molecular weight.

The transition is well illustrated in Figure 7 by the data of Kotaka, et al. (*12*) for polystyrene in toluene at various concentrations and two molecular weights. Each concentration and molecular weight approaches a different plateau level at low shear rates but all of the data approach the same linear relationship at high shears. The transition occurs at higher shear rates for lower concentrations and lower molecular weights as would be expected. Also the transition is very broad at high concentrations but is quite sharp at low concentrations. These data confirm quite well the existence of a transition from diffusion controlled stress relaxation to shear controlled stress relaxation.

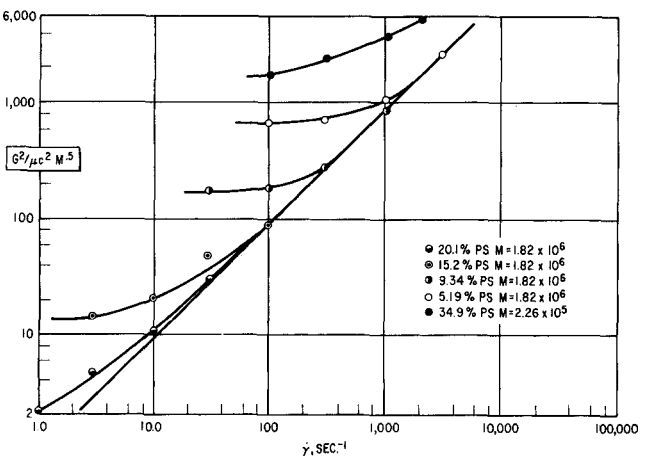

Fig. 7. Transition from diffusion controlled relaxation to shear controlled relaxation. Data from Kotaka, et al. (*12*) for solutions of polystyrene in toluene.

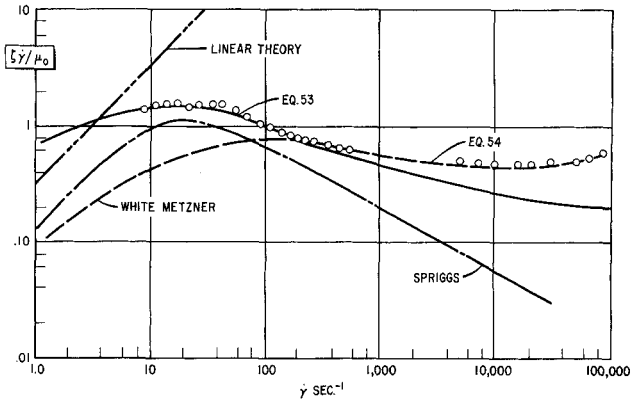

Fig. 8. Comparison of constitutive equations with 0.50% HEC data. Predictions of the reduced first normal stress difference.

Prediction of the First Normal Stress Difference

The predictions of the molecular entanglement model and a number of other constitutive equations were compared with the data for the reduced first normal stress difference. The reduced first normal stress difference is a dimensionless group obtained by dividing the first normal stress difference by the shear rate and the zero shear viscosity. The data for the 0.50% HEC are illustrated in Figure 8. Superimposed on this plot are the predictions of linear theory, the White-Metzner model, the Spriggs model, and the proposed molecular entanglement model. The linear theory, of course, is not valid at high shear rates, in this case above shear rates of 10 sec.$^{-1}$ The Spriggs model yields reasonable predictions at moderate shear rates but becomes progressively worse at shear rates above 100 sec.$^{-1}$. The Spriggs model constants were evaluated from the viscosity data. Somewhat better fit to the normal stress data could be obtained if both stress functions were fit simultaneously. The White-Metzner model is good at shear rates above 300 sec.$^{-1}$ as it is equivalent to the constant entanglement density model of Equation (54). However, it is not as satisfactory as the Spriggs model at low shear rates if the high shear rate constant is employed. The proposed entanglement model yields good predictions at all shear rates for which data were obtained. In the calculation, the constant K_R was evaluated from the data and the break point between Equations (53) and (54) was obtained from Figure 3 rather than calculated from Equation (55). Equations (53) and (54) cannot describe the lower Newtonian limit but the lower range of application can be estimated from Equation (61).

Figures 9 and 10 show the data for the 0.25 and 0.50% polyacrylamide solutions along with the predictions of the various models. The linear theory is applicable only at shear rates much below those studied. Spriggs model again diverges from the data quite rapidly at high shear rates. The White-Metzner model is good at shear rates above

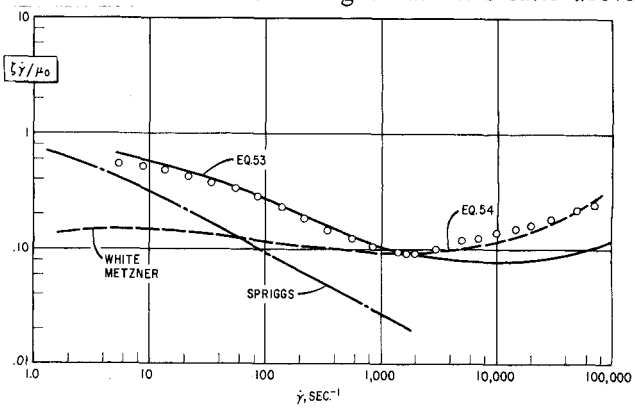

Fig. 9. Comparison of constitutive equations with 0.25% PAA data. Predictions of the reduced first normal stress difference.

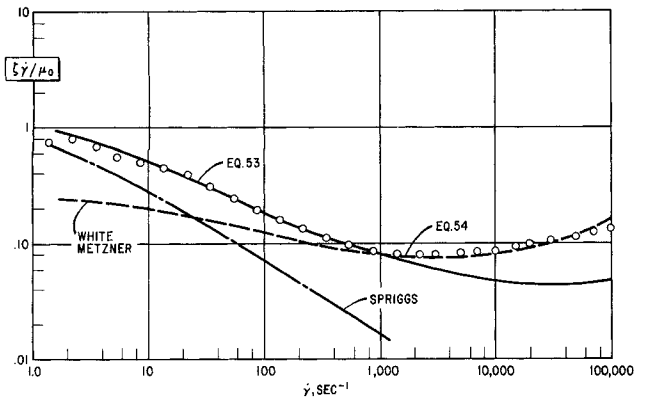

Fig. 10. Comparison of constitutive equations with 0.50% PAA data. Predictions of the reduced first normal stress difference.

1,000 sec.$^{-1}$ but is poor at low shear rates. Equations (53) and (54) yield adequate predictions over the entire shear rate range.

The Significance and Limitations of the Effective Entanglement Theory

In any theory of rheological response using the Maxwell element as a basis, the crucial parameter of interest is the natural relaxation spectrum and how this spectrum is affected by shear. For each relaxation time in the spectrum there are two associated parameters. These are the number of elements having that relaxation time and the spring constants of the individual elements. In this model it was assumed that the relaxation spectrum at any given deformation rate could be characterized by its mean value and associated with the mean value was an effective number of elements with spring constant kT. Experimentally, the effects of variation in number of elements and the spring constants cannot be separated. The polymer molecules are not ideal springs so that the spring constants are not constant at large deformations. However, the separation in this model allows the calculation of an effective number of entanglements that act like permanent crosslinks at the deformation rate in question. Certainly at zero shear rate there are many entanglements and interactions between the molecules present, but the stresses at the junctions are relaxed by the Brownian motion of the polymer molecules so that the number of effective entanglements is zero. There may be one hundred different interactions contributing to one of the so-called "effective entanglements."

When a state is reached such that a network of effective entanglements exists, either molecular breakage or aggregation of molecules is the required result. It appears that in the systems studied, aggregation was the lower energy alternative as permanent degradation was not observed until extremely high shear rates much above the break point in the rotation rate function curve. The aggregation continues as the shear rate is increased and the effective entanglement density is maintained approximately constant. Therefore, the White-Metzner equation which treats the entanglement density as a constant yields good predictions at high shear rates. The excellent fit of the White-Metzner equation has not been observed before partly because high shear rate normal stress data have been lacking and partly because if the equation is fit to the low shear rate data, the high shear rate data are not described well.

Some of the assumptions employed to simplify the proposed model are indeed questionable. In particular, the assumption that all the relaxation times in the spectrum are affected by shear in the same way. Recent experiments (*3, 19*) have indicated that shear removes the long time relaxation elements but does not affect the shorter time elements. This conclusion has a solid basis on physical grounds. However, when only the steady shear properties are considered, it appears that the net effect on the mean relaxation time caused by the two mechanisms is not significantly different.

It should be emphasized that the model cannot be expected to apply to situations other than steady shear. To adequately describe transient behavior several changes will be necessary. The spectrum of relaxation times must be retained rather than use of expected values of the moments. The transition from diffusion controlled relaxation to shear controlled relaxation will have to be adequately described within the framework of a general constitutive equation. Finally, and most difficult, the differential equations for entanglement formation and breakage will have to be formulated in a more general manner so that they can be incorporated in the original tensorial formulation.

Further work is required in steady shear analysis. The effects of molecular weight distribution on the critical entanglement density have not been well defined and are probably significant. The second normal stress difference has not been described. To obtain predictions of this quantity, a second integral must be added to the original formulation (*26*). The suggested concept of a constant entanglement density in the high shear rate regime is a gross oversimplification. Some work has been done on the formation of aggregates (*15* to *17*) and more is required, possibly from a thermodynamic point of view.

SUMMARY AND CONCLUSIONS

The Thrust Jet as an Instrument for Measuring Normal Stresses

The successful connection of the low shear rate normal stress data obtained from the rheogoniometer and the high shear rate data from the thrust jet indicate that reliable normal stress data can be obtained from the thrust jet. However, the range of the instrument is severely limited. Data cannot be obtained on low viscosity solutions because of the turbulence generated at shear rates high enough to measure the thrust. Materials must be highly elastic to be able to accurately measure the decrease in thrust caused by the elasticity. However, materials which are too elastic cause a flow instability which causes pulsing through the tube and decreases the accuracy of the thrust reading. This was becoming a problem on the 0.50% PAA solution and at higher concentrations would probably yield unreliable readings. Other instruments which can measure normal stresses at high shear rates are not available so that the thrust jet, with all of its limitations, may become a useful tool due to lack of competition.

Constitutive Theory for Polymer Solutions

The theory presented in this paper has two principal applications. Of foremost significance, the first normal stress difference can be predicted over a wide range of shear rates using the viscosity function and one additional constant that depends only on the molecular species. Secondly, the analysis is of considerable aid in elucidating the mechanisms which control the rheological behavior of polymer solutions at various shear rates. By plotting the rotation rate function, one can determine in which of three significantly different shear rate ranges one is operating:

1. Low shear rates where the controlling mechanism of stress relaxation is segmental diffusion of the polymer molecules. The number of segments and their relaxation times are natural constants for the material and independent of shear rate so that this region is characterized by a constant viscosity and first normal stress difference coefficient. This region is terminated when the reciprocal of the shear rate is of the order of magnitude of the longest of the natural relaxation times of the solution.

2. Moderate shear rates where the rheological behavior is characterized by individual polymer molecules rotating in the shear gradient and the controlling mechanism of stress relaxation is the effect of shear on the intermolecular entanglements. This region is terminated when the entanglements form a network throughout the solution that will not yield without gross changes in molecular orientation.

3. High shear rates where the individual molecules aggregate together into supermolecular units rotating in the shear gradient. These aggregates grow and become more compact with increasing shear rate.

Much theoretical work is required to extend the concepts employed in this steady shear analysis to more general flow situations. Experimental data for polymers of known molecular weight distribution are also needed to better define the relationships between the molecular weight distribution, the relaxation time spectrum, and the entanglement density.

NOTATION

A = cross-sectional area of tube, sq.cm.
c = Spriggs model constant
C = concentration of polymer, g./cc.
E = expected value operator
$f(\dot{\gamma}^2)$ = function describing effect of shear on relaxation time
F = force, dyne
$g(\dot{\gamma}^2)$ = function describing effect of shear on number of entanglements
G = shear modulus $= \tau_{12}^2/\tau_{11} - \tau_{22}$, dyne/sq.cm.
k = Boltzmann constant 1.41×10^{-19}, g.cm./°K.
k_F = constant in Equation (39)
K = constant in various equations
K'_s = Spring constant of Maxwell element $s = K_s g_s(\dot{\gamma}^2)$
K_M = constant in White-Metzner Equation (8)
K_R = constant in Equations (53) and (54)
L = tube length, cm.
L_2 = second invariant $= \dot{\gamma}^2$ in steady shear
M = average molecular weight
n = power law parameter
n' = $d\ln\tau_{12}/d\ln(8V/D)$
N_{Av} = Avogadro's number 6.03×10^{23} molecules/mole
N_M = number of molecules/cc.
N_0' = total number of entanglements/cc. $= N_0 g(\dot{\gamma}^2)$
N'_s = number of entanglements of relaxation time λ_s/cc. $= N_s g(\dot{\gamma}^2)$
p_0 = isotropic pressure, dyne/sq.cm.
P_{ij} = deviatoric stress components, dyne/sq.cm.
r = radial distance, cm.
R = radius of thrust tube; radius of polymer molecule, cm.
s = subscript indicating relation to particular relaxation time λ_s
t = time, sec.
t = $t - t_0$ time since origination of element, sec.
T = thrust, g.; temperature, °K.
T_N = Newtonian thrust $= 4/3\ \pi\ \rho\ V^2\ R^2$
u = local velocity, cm./sec.
V = average velocity, cm./sec.
$V(\dot{\gamma}^2)$ = rotational velocity of molecule, cm./sec.
$Z(\alpha)$ = Riemann ζ function

Greek Letters

α = Ellis model parameter
β = second normal stress difference coefficient, g./cm.
$\dot{\gamma}$ = shear rate, sec.$^{-1}$
$\dot{\gamma}_B$ = shear rate at which an effective network is formed
δ^{ij} = Kronecka delta
ϵ = Spriggs model parameter
ζ = first normal stress difference coefficient, g./cm.
λ = relaxation time, sec.
λ'_s = relaxation time of element $s = \lambda_s f_s(\gamma^2)$, sec.
λ_E = effective relaxation time, sec.
μ = viscosity, g./cm.sec.
μ_0 = zero shear rate viscosity, g./cm.sec.
μ_s = solvent or infinite shear rate viscosity, g./cm.sec.
ν = effective entanglement density, entanglements per molecule
π = 3.1416
ρ = density, g./cc.
τ_{ij} = components of stress tensor, dyne/sq.cm.
τ_{12} = shear stress, dyne/sq.cm.
$\tau_{11} - \tau_{22}$ = first normal stress difference, dyne/sq.cm.
$\tau_{22} - \tau_{33}$ = second normal stress difference, dyne/sq.cm.
Φ = statistical parameter defined by Equation (37)
$\psi(\overline{t}, L_2)$ = relaxation function
$\omega(\gamma^2)$ = rotation rate function, sec.$^{-1}$

LITERATURE CITED

1. Bogue, D. C., and J. O. Doughty, *Ind. Eng. Chem. Fundamentals*, **5**, 243 (1966).
2. ———, *ibid.*, **5**, 253 (1966).
3. Booij, H. C., *Rheologica Acta*, **5**, 215 (1966).
4. Bueche, F., "Physical Properties of Polymers," *Interscience*, New York (1962).
5. ———, *J. Chem. Phys.*, **22**, 1570 (1954).
6. Coleman, B., and W. Noll, *Arch. Rat. Mech. Anal.*, **3**, 289 (1959).
7. *Ibid.*, **6**, 355 (1960).
8. Flory, P. J., "Principles of Polymer Chemistry," Cornell Univ. Press, Ithaca, N. Y. (1953).
9. Gillespie, T., *J. Colloid Int. Sci.*, **22**, 133 (1966).
10. Greensmith, H. W., and R. S. Rivlin, *Phil. Trans. Roy. Soc., London*, **A245**, 399 (1953).
11. Huppler, J. D., Ph.D. thesis, Univ. Wisconsin, Madison (1965).
12. Kotaka, T., M. Kurato, and M. Tamura, *Rheologica Acta*, **2**, No. 2, 179 (1962).
13. Lodge, A. S., "Elastic Liquids," Academic Press, New York (1964).
14. ———, *Trans. Faraday Soc.*, **52**, 120 (1956).
15. Lund, J. K., and H. A. Pohl, *Can. J. Chem. Eng.*, **43**, 231 (1965).
16. Mooney, M., *J. Applied Phys.*, **27**, 691 (1956).
17. ———, *J. Polymer Sci.*, **34**, 599 (1959).
18. Oldroyd, J. G., *Proc. Royal Soc.*, **A200**, 523 (1950).
19. Osaki, K., M. Tamura, M. Kurata, and T. Kotaka, *J. Phys. Chem.*, **60**, 4183 (1965).
20. Pao, Y. H., *J. Polymer Sci.*, **61**, 413 (1962).
21. Rouse, P. E., *J. Chem. Phys.*, **21**, 1272 (1953).
22. Shertzer, C. R., M.Ch.E. thesis, Univ. Delaware, Newark, (1964).
23. Shertzer, C. R., and A. B. Metzner, *Trans. Plast. Inst.*, **31**, 148 (1963).
24. Spriggs, T. W., *Chem. Eng. Sci.*, **20**, 931 (1965).
25. ———, and R. B. Bird, *Ind. Eng. Chem. Fundamentals*, **4**, 182 (1964).
26. ———, J. D. Huppler, and R. B. Bird, *Trans. Soc. Rheology*, **10**, Part 1, 191 (1966).
27. Takemura, T., *J. Polymer Sci.*, **27**, 549 (1958).
28. Tanner, R. I., and J. M. Simmons, *Chem. Eng. Sci.*, to be published.
29. Tobolsky, A. V., "Properties and Structure of Polymers," John Wiley, New York (1960).
30. White, J. L., M. Ch.E. thesis, Univ. Delaware, Newark (1962).
31. White, J. L., and A. B. Metzner, *J. Appl. Polymer Sci.*, **7**, 1867 (1963).
32. Williams, M. C., Ph.D. thesis, Univ. Wisconsin, Madison (1964).
33. ———, and R. B. Bird, *Phys. of Fluids*, **5**, 1126 (1962).
34. Zimm, B. H., *J. Chem. Phys.*, **24**, 269 (1956).

Manuscript received November 29, 1967; revision received May 16, 1968; paper accepted May 20, 1968. Paper presented at AIChE New York City meeting.